

Effect of Microstructural Characteristics on Mechanical Properties of Austenitic, Ferritic, and γ - α Duplex Stainless Steels



MITSUHIRO OKAYASU and DAIKI ISHIDA

Materials properties of γ (austenite), α (ferrite), and γ - α duplex stainless steels were experimentally examined using samples with different grain sizes (8 to 1000 μm) and different ratios of the γ to α phase (γ proportion: 35 to 78 pct). The mechanical properties (hardness and tensile strength) of the duplex stainless steel were about 1.5 times higher than those of the austenitic and ferritic stainless steels. Two main reasons for the high strength of duplex stainless steel were identified as follows: (i) severe interruption of slip deformation in the γ phase on the α phase; (ii) a high misorientation angle around phase boundaries between the γ and α phases, caused by bonding of the different lattice structures: γ -fcc and α -bcc. The ultimate tensile strength of duplex stainless steel increased with increasing proportion of the γ phase to 50 pct, but decreased with a further increase in the amount of γ phase. The mechanical properties improved with decreasing grain size of the stainless steels, which follows the Hall-Petch relationship; however, the reverse relationship was obtained for ferritic stainless steel, especially with large grain sizes (100 to 1000 μm), in which the size of hard Cr_{23}C_6 precipitates increased with increasing grain size.

<https://doi.org/10.1007/s11661-018-5083-4>

© The Minerals, Metals & Materials Society and ASM International 2019

I. INTRODUCTION

STAINLESS steels have been employed around the world in various engineering applications, such as for hydraulic turbines and high-pressure pipes in power plants. This is due to their excellent materials properties of high strength, high toughness, and high corrosion resistance. There are several conventional stainless steels, including austenitic, ferritic, and martensitic stainless steels. One typical property of austenitic stainless steel (AS) is its non-magnetic characteristics, although this property is altered as the stainless steel is deformed severely, *i.e.*, strain-induced martensite formation occurs. This phenomenon not only induces magnetic properties, but also results in low formability caused by the hardened martensite structure. After the forging process, stainless steels are used to make a specific shape, so changes of materials properties have to be considered in the design of their engineering applications. To date, several stainless steels have been proposed with improved mechanical properties. A

nanocrystalline 316L austenitic stainless steel was produced, in which the fine microstructure gave an extremely high yield strength of up to 1450 MPa.^[1] The influence of the delta ferrite phase on the mechanical properties of 13Cr-4Ni martensitic stainless steel was investigated, where delta ferrite did not change the upper- and lower-shelf energy of the steel, but lowered the impact energy remarkably in the transition temperature range and raised the ductile-to-brittle transition temperature.^[2] The tensile properties of SUS316L stainless steel, fabricated using the laser engineered net shaping (LENS) technique, were examined. The resulting unusual distinct dual-phase microstructure of the LENS-SUS316L resulted in high levels of the yield stress (YS) and ultimate tensile strength (UTS) of 527 and 740 MPa, respectively.^[3]

Ferritic stainless steels (FS), consisting of 16 to 18 Cr and 0.12 C (SUS430), are widely used, such as for bathtubs and kitchenware; however, the mechanical properties of SUS430 are apparently lower than those of SUS304. To improve the hardness and corrosion resistance of FS, surface coatings created by physical vapor deposition (PVD) have been employed.^[4] High-strength FS has been generated using the equal channel angular extrusion technique, where total strain, *e.g.*, of 2.3, was implemented using the extrusion process at room temperature. The tensile strength of the extruded FS increased significantly, which was caused by the high dislocation density.^[5] Although the mechanical

MITSUHIRO OKAYASU and DAIKI ISHIDA are with the Graduate School of Natural Science and Technology, Okayama University, 3-1-1 Tsushimanaka, Kita-ku, Okayama 700-8530, Japan. Contact e-mail: mitsuhiro.okayasu@utoronto.ca

Manuscript submitted August 20, 2018.

Article published online January 1, 2019

properties of SUS430 have been examined, there is no clear information concerning the relationship between the microstructural characteristics and mechanical properties.

In recent years, duplex stainless steels (DS), comprising both austenite and ferrite phases, have received special attention because of their good mechanical properties and high corrosion resistance.^[6] The relative amounts of ferrite and austenite in the DS are important to determine the combination of mechanical properties and corrosion resistance.^[7] Sahu *et al.* examined the effect of 475 °C embrittlement on the mechanical properties of DS, reaching the conclusion that the change in mechanical properties of DS occurs at 475 °C when compared with binary iron-chromium systems, due to their brittleness. Duplex stainless steels are considered to be recrystallized by the heating process, which is a dissimilar characteristic of the constituents of their microstructure, ferrite and austenite.^[8] In the temperature range 300 °C to 1050 °C, severe phase transformation occurs. Mateo *et al.*^[9] have investigated the characterization of the intermetallic G-phase in an AISI duplex stainless steel, where the duplex austenite-ferrite stainless steels are aged within the intermediate range of temperatures (250 °C to 500 °C). One of these phenomena is the precipitation of the intermetallic G-phase. Such changes of the phase characteristics provide different toughness and corrosion behaviors.^[10,11] Although several academic papers have been published that interpret the material properties of DS, there is an apparent lack of related information. In particular, the mechanical properties of DS can be examined by changing the ratio of the austenite to ferrite components; furthermore, the resulting mechanical properties can be analyzed using other conventional stainless steels, such as FS and AS. The aim of this work was therefore to investigate the influences of the grain size and phase characteristics on the mechanical properties of DS using various stainless steels.

II. EXPERIMENTAL PROCEDURES

A. Material Preparation

The present work used several cold-rolled stainless steel plates, supplied by Nippon Steel & Sumitomo Metal Corp, Japan, *i.e.*, austenitic (SUS304L: AS), ferritic (SUS430: FS), and duplex (SUS821L1: DS) stainless steels. Because DS consists of austenite and ferrite phases, conventional AS and FS were used for comparison of their materials properties. Thickness of the cold-rolled steel sheets was about 3 mm. The

chemical compositions of the three steels are listed in Table I.

To examine the effect of microstructural characteristics on the mechanical properties, the grain size of the steels was regulated to within similar sizes by various heat treatments. Based on the grain size of the AS sample, annealed at 420 °C for 1 hours, the grain sizes of the FS and DS samples were regulated using the following conditions: 800 °C for 5 hours (FS) and 1100 °C for 15 hours (DS). Furthermore, to understand the influence of the microstructural characteristics in detail, the effects of grain size of FS and γ/α ratio of DS on the mechanical properties were examined, where the microstructures were controlled by the heating process: 800 °C to 1100 °C for about 2.5 hours (FS) and 1100 °C for 1 to 15 hours (DS).

The mechanical properties of the stainless steels were determined from hardness and tensile tests. For the tensile tests, a rectangular dumbbell-shaped specimen of 12 mm × 2.5 mm × 1 mm was employed. Tensile stress was applied by a screw-driven universal testing machine with a capacity of 50 kN. The test specimens were loaded at a rate of 1 mm/min until final failure. The engineering tensile strength and engineering strain were measured using a commercial load cell and strain gauge, respectively. Those data were monitored and recorded *via* a data acquisition system in conjunction with a computer.

Magnetic flux density (MFD) measurements and electron backscatter diffraction analysis (EBSD) were executed to clarify the phase characteristics. In this case, the influence of the ratio of the γ phase to α phase on the MFD value was examined. The MFD was measured using a Tesla meter with a resolution of 0.01 mT. The EBSD analysis was executed with an accelerating voltage of 15 kV using a scanning electron microscope and its related software.



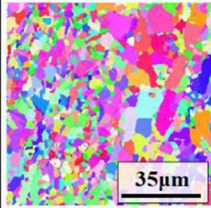


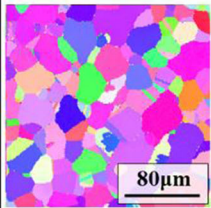
III. RESULTS AND DISCUSSION

A. Austenite, Ferrite, and γ - α Duplex Stainless Steels

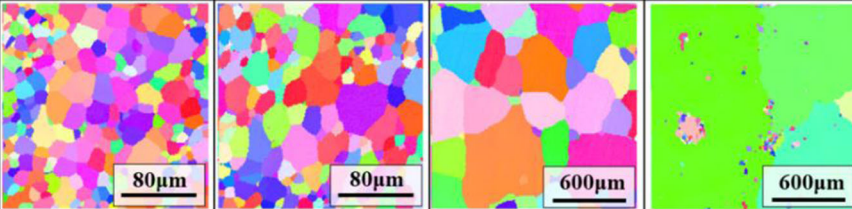
Figure 1 shows the inverse pole figure (IPF) maps for the various stainless steels: (a) AS, FS, and DS with and without grain regulation; (b) FS with different grain sizes, and (c) DS with different γ/α ratios. In Figure 1(a), three stainless steels with similar grain sizes of about 20 μm and different sizes (4.6 to 22.3 μm) are observed. For the FS sample shown in Figure 1(b), the grain size was altered to within the range 13.7 to 1006 μm . From Figure 1(c), the DS samples show γ and α phases at different ratios from 45.7 to 76.4 pct of the γ phase.

Table I. Chemical Compositions of the Austenitic (SUS304L), Ferritic (SUS430), and Duplex Stainless Steels (SUS821L1)

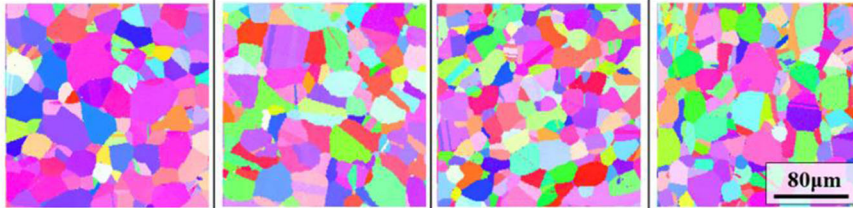
	C	Si	Mn	P	S	Ni	Cr	Mo	Cu	N
AS	0.02	0.70	1.49	0.03	0.002	10.8	18.3	—	—	—
FS	0.04	0.24	0.32	0.23	0.00	0.08	16.1	—	—	—
DS	0.02	0.29	3.22	0.02	0.0002	2.13	20.9	0.27	1.04	0.16

	AS	FS	DS
	As-received		
			
GS (Grain size)	22.3 μm	11.3 μm	4.6 μm
	After grain size regulation		
			
GS	22.3 μm	15.8 μm	20.9 μm

(a) AS, FS and DS

				
	GS	13.7 μm	15.8 μm	276.5 μm

(b) FS

				
	γ ratio	45.7 %	54.0%	59.3%

(c) DS

Fig. 1—Inverse pole figure (IPF) maps for three stainless steels as-received and with regulated grain size: (a) austenitic, ferritic, and duplex stainless steels, (b) ferritic stainless steel, and (c) duplex stainless steel.

To substantiate the variation of the amount of γ phase, the magnetic properties were investigated, because the amount of α phase is related to the extent

of MFD. Figure 2 shows the variation of MFD as a function of the γ/α ratio. The MFD value decreased linearly with increasing proportion of the γ phase. From

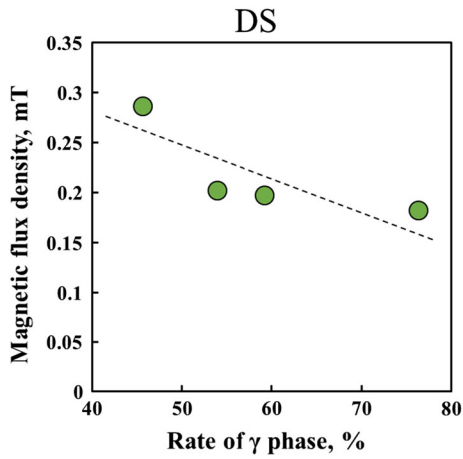


Fig. 2—Variation of magnetic flux density as a function of proportion of γ phase in duplex stainless steel.

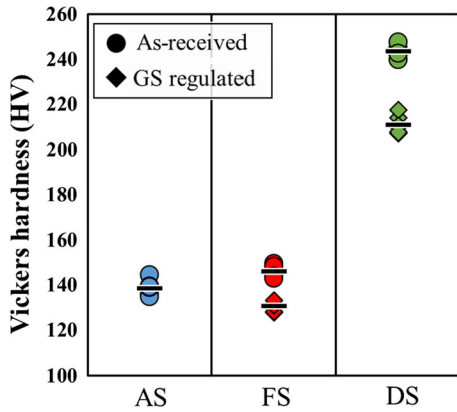


Fig. 3—Variation in Vickers hardness of three stainless steels with and without grain regulation.

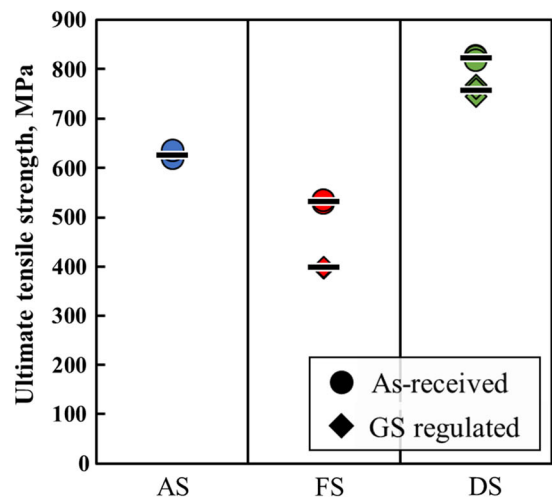
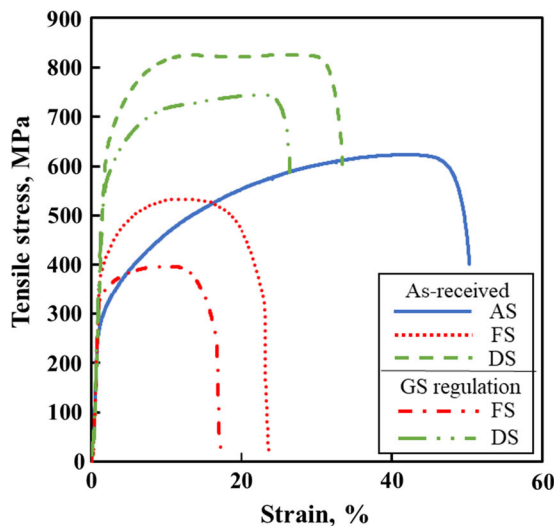


Fig. 4—Engineering tensile stress–strain curves and their tensile properties for three stainless steels.

these microstructural characteristics, the different mechanical properties could be obtained. (K-3) Wei *et al.* have reported that ultrafine grain with face-centered cubic (fcc) and body-centered cubic (bcc) structures make change of the mechanical properties,^[12] *i.e.*, the material strength is attributed to the lattice structure due to the different close-packed structure.

Figure 3 indicates the Vickers hardness of the three stainless steels before and after the grain regulation. Note that there are no data plots of AS for the grain regulation, as the grain size for the stainless steels was designed on the basis of the AS sample. It is clear that high hardness was obtained for DS, exceeding 200 HV, although the hardness of AS and FS was as low as 140 HV, which is similar to that of the associated stainless steel reported in previous work of about 160 HV.^[13] The hardness of the DS and FS samples decreased after grain regulation, due to the enlarged grain size. Despite the low hardness similarly observed for AS (γ) and FS (α), high hardness was obtained for DS ($\gamma + \alpha$). The reason for this cannot be interpreted solely based on the grain size; other factors, such as phase characteristics, could be influencing this behavior. This is discussed in the later section of this paper.

Figure 4 shows representative stress–strain curves for the stainless steels with and without grain regulation. The tensile strength for DS and FS decreased after grain regulation, which was similar to the hardness test results. The UTS of DS was higher than that of AS and FS, although the UTS of AS was slightly higher than that of FS. Low UTS and the low ductility were obvious for FS and relatively high UTS with high ductility was seen for AS. In contrast to the hardness results shown in Figure 3, the tensile properties of AS and FS showed different tendencies: the relatively high UTS with low yield strength of AS is affected by severe work hardening and strain-induced martensite. Shakhova *et al.* examined the variation of hardness of AS, where the hardness value increased by a factor of three at about $\epsilon = 3.5$.^[13] Consideration should be given to

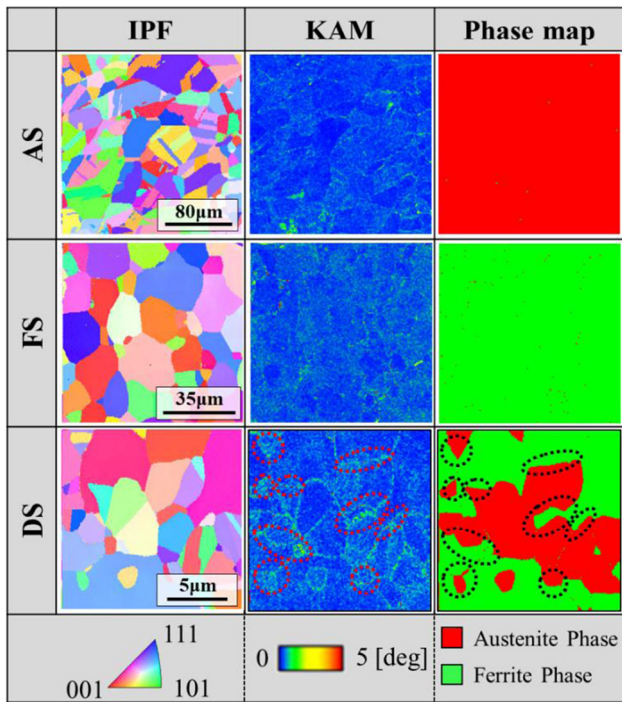


Fig. 5—Inverse pole figure (IPF), Kernel average misorientation (KAM), and phase maps for duplex stainless steel.

whether the phase characteristics affect hardness in DS samples.

Figure 5 shows the IPF, KAM (Kernel average misorientation), and phase maps for the DS together with AS and FS. The austenite and ferrite phases are clearly observed for the three stainless steels. Interestingly, unlike AS and FE, high misorientation of about 3 deg was detected in the DS sample around the phase boundaries between the γ and α phases, as identified by the dashed circles. Such high misorientation may cause high internal strain, resulting in the high UTS of DS.^[14] In this case, the high internal strain may be affected by bonding of the different lattice structures: close-packed γ -fcc (0.257 nm) and α -bcc (0.248 nm), (K-3) which lead to the high resistance of the dislocation activity in DS around the phase boundaries.

To understand the mechanical properties of the three stainless steels in details, failure analysis was carried out. Figure 6 displays scanning electron micrographs showing fracture surfaces of the AS, FS, and DS samples after tensile testing. The failure patterns of the AS and DS samples were similar, where dimple and slip-based failure modes are seen in the middle and at the edge of the fracture surface, respectively. Although dimples are seen in the fracture surface of FS, their size is smaller. This would be affected by the low ductility of the FS sample.

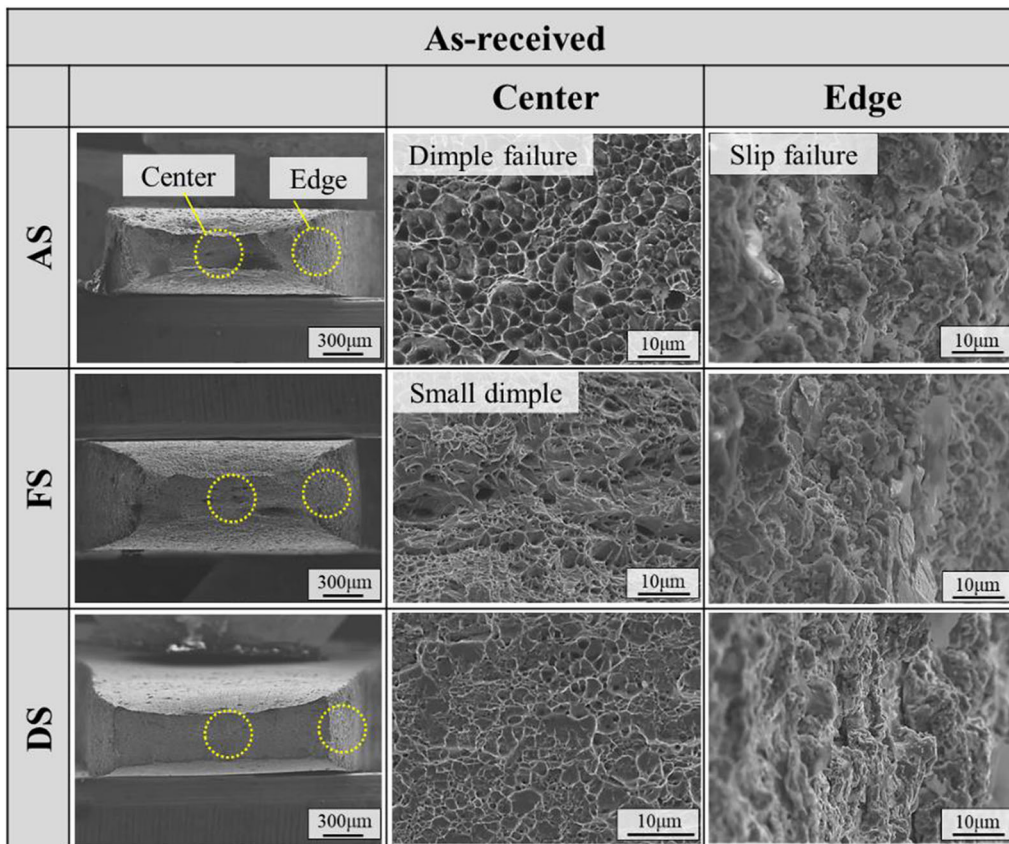


Fig. 6—Scanning electron micrographs of fracture surfaces of austenitic, ferritic, and duplex stainless steels after tensile testing.

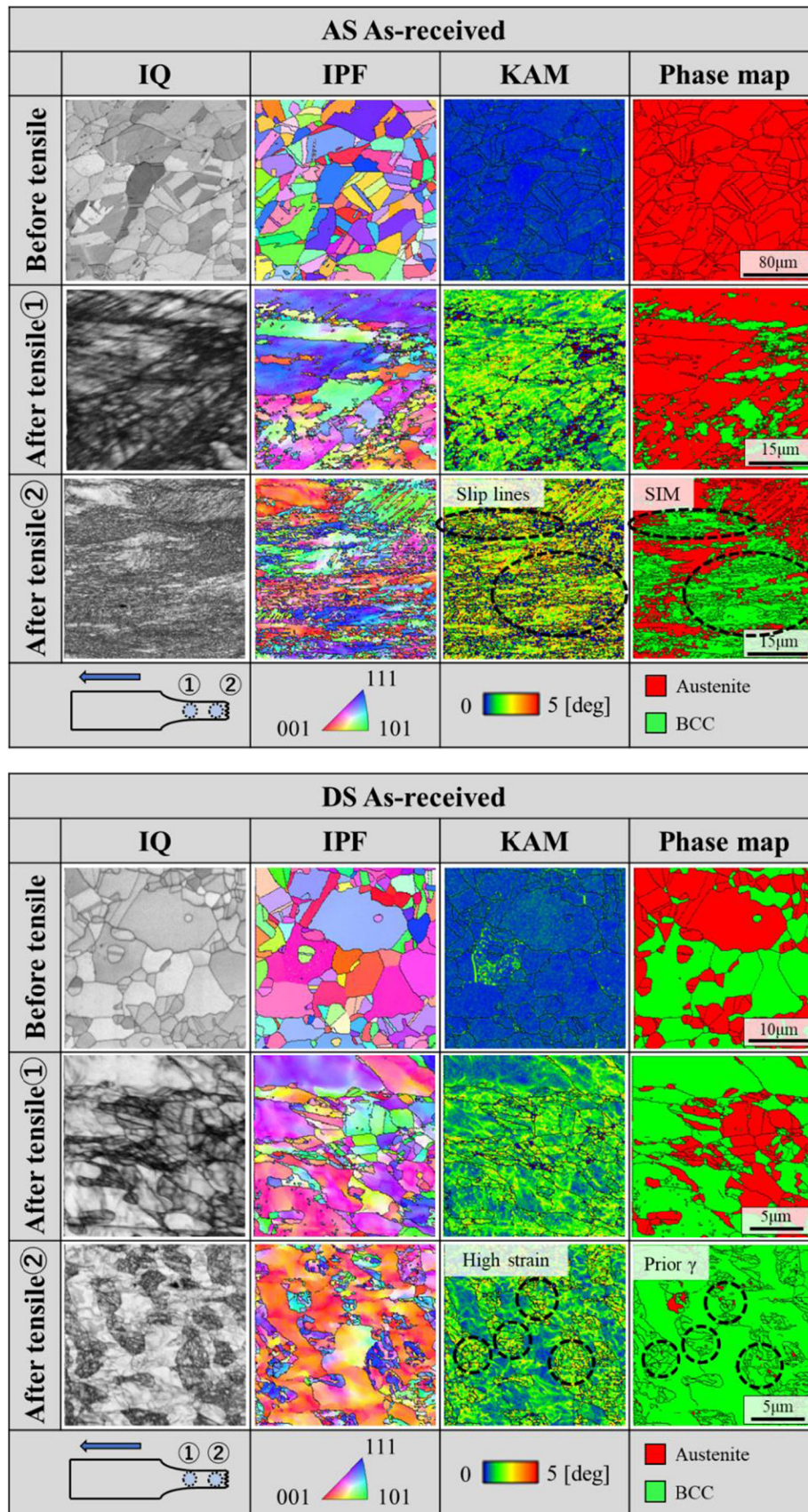


Fig. 7—Inverse pole figure (IPF), Kernel average misorientation (KAM), and phase maps for ferritic and duplex stainless samples before and after tensile testing.

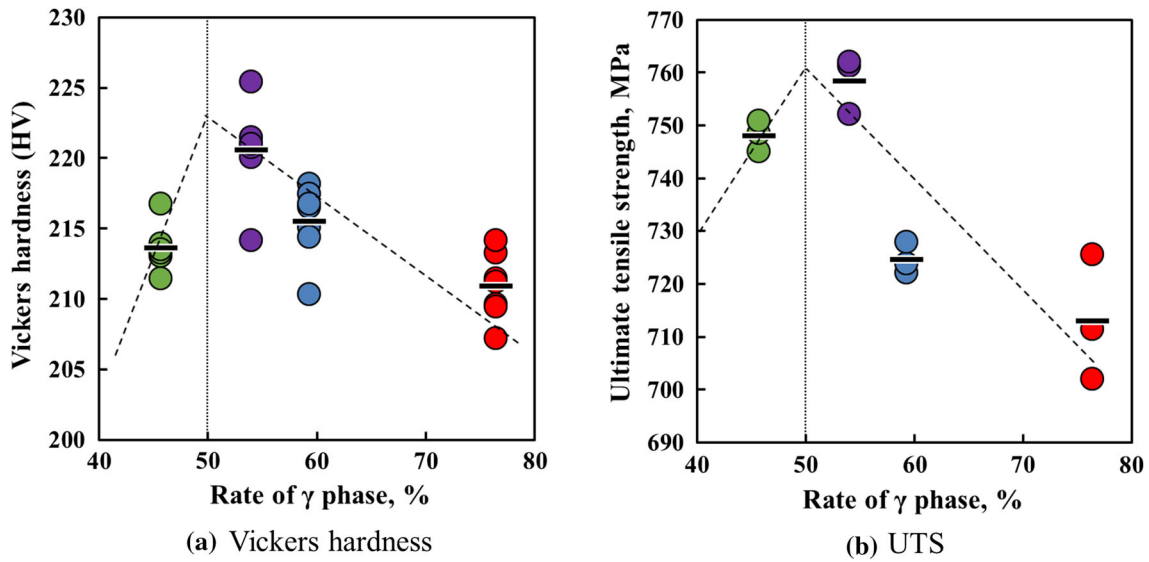


Fig. 8—Variation of materials properties as a function of proportion of γ phase for duplex stainless steel: (a) Vickers hardness and (b) ultimate tensile strength.

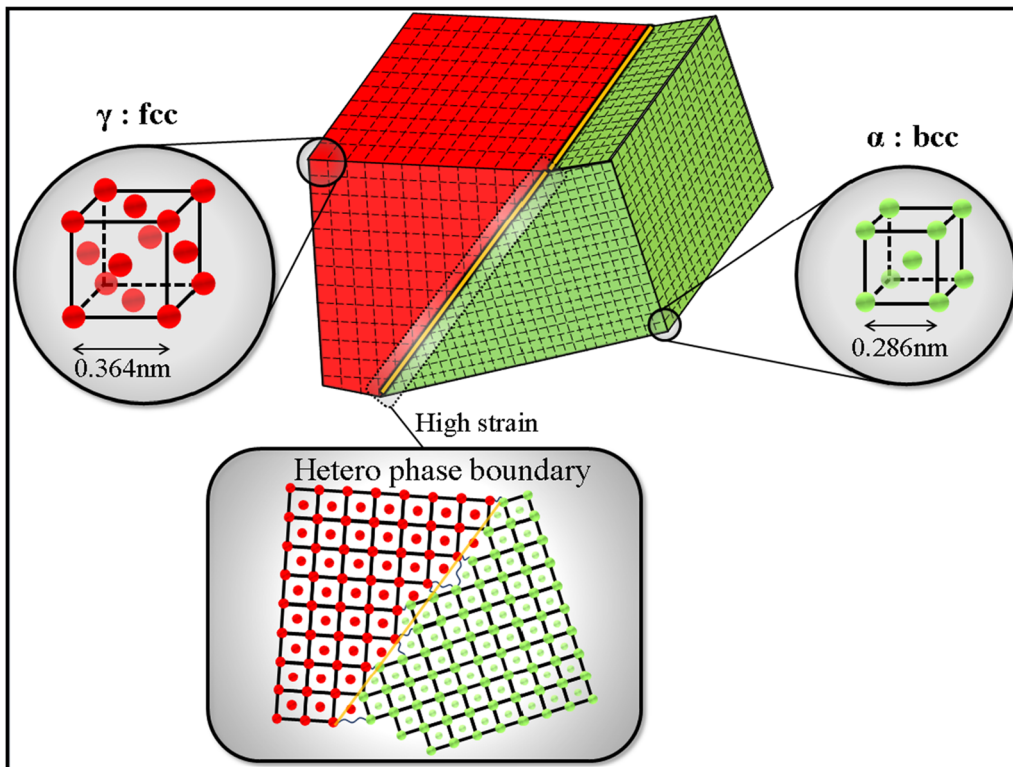


Fig. 9—High strength models for duplex stainless samples.

The failure characteristics were further analyzed to interpret the good mechanical properties of DS. Figure 7 shows the IPF, KAM, and phase maps of cross sections of the AS and DS samples near and far from the fracture surface. It is obvious from both the IPF and KAM maps that the severity of strain increased after tensile testing, especially near the fracture surface.

It is clear that the strong texture of γ -fcc for AS and γ -fcc and α -bcc for DS changed after the tensile test, during which the total area fraction of α -bcc increased to 59 pct for AS and 98 pct for DS, attributed to strain-induced martensite formation. It should be pointed out that the α -bcc structure for AS and DS is related to that of α' -bcc for AS and α -bcc and α' -bcc for DS. It has been

reported that AS (SUS304) at the fracture point consisted of about 50 pct α' -bcc near the fracture surface after tensile testing,^[15] which is close to that measured for our SUS304L sample, *i.e.*, about 59 pct. Owing to the technical difficulty of distinguishing between α -bcc (ferrite) and α' -bcc (martensite) by EBSD analysis, the extent of strain-induced martensite could not be clarified for DS. However, in this case, the rate of α' -bcc conversion may be approximated: the area fraction of γ -fcc in DS was about 55 pct before the tensile test, indicating that the phase structure of α' -bcc after the tensile test could be about 53 pct, *i.e.*, 55 pct (γ -fcc before tensile test) – 2 pct (γ -fcc after test) = 53 pct (α' -bcc).

From the IPF and KAM maps as shown in Figure 7, the strain characteristics for AS and DS differed after the tensile test: severe strain occurred in AS due to a large number of slip lines and high KAM value; in contrast, a severely strained area was observed in limited regions of the DS sample, as indicated by the dashed circles, *e.g.*, γ -fcc, while other areas did not have severe

deformation, *e.g.*, α -bcc. In this case, the tiny limited regions were related to the areas in which strain-induced martensite transformation from γ -fcc to α' -bcc occurred. From the DS strain characteristics, slip deformation occurred severely in γ -fcc, but could be interrupted by the presence of α -bcc, leading to high tensile strength.

B. Effect of γ and α Phases on Mechanical Properties

The influence of the γ -fcc and α -bcc phases on the material properties of the DS was investigated. Despite heating the sample to 1100 °C, the Cr_{23}C_6 precipitate was not detected, unlike the FS sample, because of the different chemical composition. Figure 8 shows the variation of (a) Vickers hardness and (b) UTS as a function of the γ/α ratio. Both mechanical properties increased with increasing area fraction of the γ phase to 50 pct, but decreased with further increase in the proportion of γ phase, *i.e.*, the best mechanical properties of DS were obtained at 50 pct of the γ phase. Such high mechanical properties can be interpreted in terms of the severe internal strain around phase boundaries and interruption of slip in the γ phase by the α phase, as shown in Figures 5 and 7, respectively. Figure 9 displays the high strength models for duplex stainless samples. As seen, the severe strain could generate in the duplex stainless steels adjacent to the phase boundaries because of the different size of lattice, *i.e.*, the γ phase (0.364 nm) vs the α phase (0.286 nm). Iza-Mendia *et al.* have reported that failure occurs in the duplex stainless steel at the interface of the related phases, which may affect the extent of stress concentration.^[16]

C. Effect of Grain Size on Mechanical Properties

Figure 10 shows the variation of Vickers hardness as a function of grain size of FS. Two different trends were obtained: for FS samples with small grain sizes (8 to 15 μm), the hardness increased with decreasing the grain size, *i.e.*, the Hall–Petch (H–P) relationship; for large grain sizes (100 to 1000 μm), the hardness level

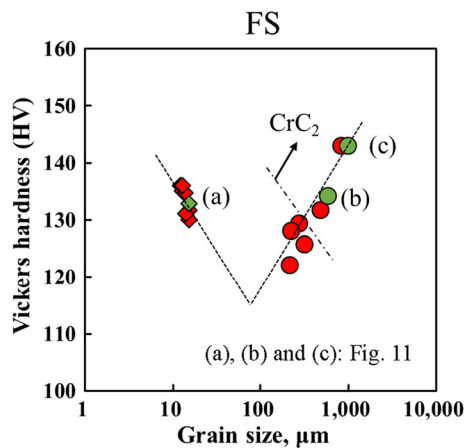


Fig. 10—Variation of Vickers hardness as a function of grain size for ferritic stainless steel.

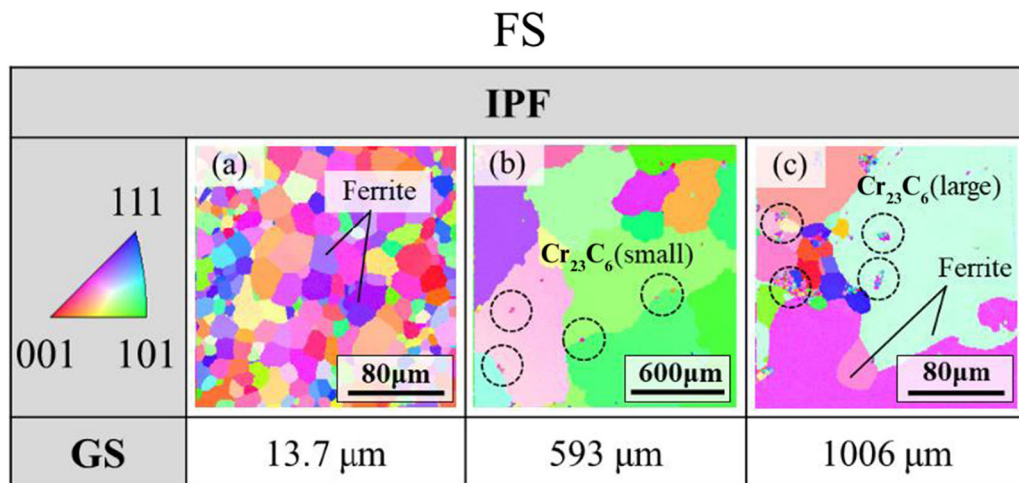


Fig. 11—Inverse pole figure (IPF) maps of ferritic stainless steels with mean grain sizes of (a) 13.7 μm , (b) 593 μm , and (c) 1006 μm , showing the different Cr_{23}C_6 precipitates.

increased with increasing grain size, *i.e.*, an inverse H–P relationship. Kashyap and Tangri reported that bi- and linear H–P relationships were obtained for the associated stainless steel, depending on the dislocation density and grain size.^[17] Moreover, such hardness profile in Figure 10 is attributed to the precipitation behavior. Sahu has examined the precipitation characteristics make change in the mechanical properties in duplex stainless steels.^[7]

To interpret the inverse H–P relationship for FS, the microstructural characteristics were analyzed. Figure 11 displays the IPF maps of FS samples with mean grain sizes of (a) 13.7 μm , (b) 593 μm , and (c) 1006 μm . Different microstructural characteristics are observed: in samples with large grains (593 μm and 1006 μm), the precipitate particles occurred in the matrix although the size of the precipitate was dependent on the grain size, *i.e.*, the larger the grain, the larger the precipitate particle; in contrast, no clear precipitate was detected in the sample with small grains (13.7 μm). From energy-dispersive spectroscopy (EDS) analysis, the precipitates were identified as Cr_{23}C_6 , which could be created by the process of heating to above 900 °C, such as for the γ loop.^[18] The Cr_{23}C_6 precipitates were eliminated in FS samples that were heated to below 900 °C (850 °C) for a certain period of time. The precipitate particles were grown by heating to the higher temperatures. As shown in Figure 10, the hardness of Sample (c) was higher than that of Sample (b): the increment of hardness in an inverse H–P relationship is attributed to the size of the Cr_{23}C_6 precipitates.

IV. CONCLUSIONS

Materials properties of austenitic, ferritic, and γ - α duplex stainless steels were experimentally investigated using samples with different microstructural characteristics. The following results were obtained.

1. In the three stainless steels with the same grain size, the hardness of the DS was about 1.5 times higher than that for the AS and FS. In contrast to the hardness results, different tensile properties were obtained: high tensile strength and high ductility were obtained for the DS, although low tensile properties were measured for FS. Relatively high tensile strength with high ductility was obtained for AS due to severe work hardening and strong strain-induced martensite.
2. The mechanical properties of the stainless steels are attributed not only to the grain size, but also to other microstructural characteristics. For the FS sample with small grain size (8 to 15 μm), the hardness increased with decreasing grain size (Hall–Petch relationship); however, the opposite

trend was obtained for large grain sizes (100 to 1000 μm), where the hardness increased with increasing grain size because of the increase in size of hard Cr_{23}C_6 precipitates.

3. High lattice misorientation of about 3 deg was detected in DS around the phase boundaries between γ -fcc and α -bcc, which is caused by different lattice structures: close-packed γ -fcc (0.257 nm) and α -bcc (0.248 nm). The high internal strain caused high mechanical strength. Severe strain in DS occurred in the γ phase, which was interrupted by the α phase. This phenomenon also contributed to improved mechanical properties. The tensile strength of DS increased with increasing proportion of the γ phase to 50 pct, but decreased with further increase in the γ phase.

CONFLICT OF INTEREST

The authors declare no conflict of interest.

REFERENCES

1. X.H. Chen, J. Lu, L. Lu, and K. Lu: *Scripta Mater.*, 2005, vol. 52, pp. 1039–44.
2. P. Wang, S.P. Lu, N.M. Xiao, D.Z. Li, and Y.Y. Li: *Mater. Sci. Eng. A*, 2010, vol. 527, pp. 3210–16.
3. M. Ziętala, T. Durejko, M. Polański, I. Kunce, T. Płociński, W. Zieliński, M. Łazińska, W. Stępniewski, T. Czujko, K.J. Kurzydłowski, and Z. Bojar: *Mater. Sci. Eng. A*, 2016, vol. 677, pp. 1–10.
4. N. Saito, M. Mabuchi, M. Nakanishi, I. Shigematsu, G. Yamauchi, and M. Nakamura: *J. Mater. Sci.*, 2001, vol. 36, pp. 3229–32.
5. C.H. Hsu, C.K. Lin, K.H. Huang, and K.L. Ou: *Surf. Coat. Technol.*, 2013, vol. 231, pp. 380–84.
6. V.S. Moura, L.D. Lima, J.M. Pardal, A.Y. Kina, R.R.A. Corte, and S.S.M. Tavares: *Mater. Charact.*, 2008, vol. 59, pp. 1127–32.
7. J.K. Sahu, U. Krupp, R.N. Ghosh, and H.-J. Christ: *Mater. Sci. Eng. A*, 2009, vol. 508, pp. 1–14.
8. W. Reick, M. Pohl, and A.F. Padilha: *ISIJ Int.*, 1998, vol. 38, pp. 567–71.
9. A. Mateo, L. Llangas, M. Anglanda, A. Redjaïmia, and G. Metauer: *J. Mater. Sci.*, 1997, vol. 32, pp. 4533–40.
10. T. Kuroda: *Trans. JWRI*, 2005, vol. 34, pp. 63–68.
11. J.O. Nilsson and A. Wilson: *Mater. Sci. Technol.*, 1993, vol. 9, pp. 545–54.
12. Q. Wei, S. Cheng, K.T. Ramesh, and E. Ma: *Mater. Sci. Eng. A*, 2004, vol. 381, pp. 71–79.
13. I. Shakhova, V. Dudko, A. Belyakov, K. Tsuzaki, and R. Kaibyshev: *Mater. Sci. Eng. A*, 2012, vol. 545, pp. 176–86.
14. J. Schiøtz, T. Vegge, F.D. Di Tolla, and K.W. Jacobsen: *Phys. Rev. B*, 1999, vol. 60, pp. 11971–83.
15. M. Okayasu, H. Fukui, H. Ohfujii, and T. Shiraiishi: *Mater. Sci. Technol.*, 2014, vol. 30, pp. 301–08.
16. A. Iza-Mendia, A. Piñol-Juez, J.J. Urcoia, and I. Gutiérrez: *Metall. Mater. Trans. A*, 1998, vol. 29A, pp. 975–86.
17. B.P. Kashyap and K. Tangri: *Acta Metall. Mater.*, 1995, vol. 43, pp. 3971–81.
18. M. Kowaka: *Zairyo*, 1974, vol. 23, pp. 924–35.